Processing and Application of Ceramics 10 [1] (2016) 47–55
DOI: 10.2298/PAC1601047A

BY-NC-ND

Structural, dielectric and conductivity studies of $LiNi_{0.75}Mg_{0.25-x}Cu_xPO_4$ synthesized by solid state reaction method

Kotamalige Anand[1], Bhajanthri Ramamurthy[1], Valaparla Veeraiah[2], Kannipamula Vijaya Babu[3,*]

[1]*Department of Instrumentation and USIC, Sri Krishna Devaraya University, Anantapur, India*
[2]*Department of Physics, Andhra University, Visakhapatnam, India*
[3]*Advanced Analytical Laboratory, Andhra University, Visakhapatnam, India*

Received 2 February 2016; Received in revised form 22 March 2016; Accepted 28 March 2016

Abstract

The olivine structured $LiNi_{0.75}Mg_{0.25-x}Cu_xPO_4$ (x = 0, 0.05 and 0.1) cathode materials were synthesized by solid state reaction method. The XRD, FTIR and FESEM studies were conducted to investigate the phase purity, crystal structure, lattice parameters and morphology, respectively. The powder X-ray diffraction studies confirmed the single phase formation of the pure and doped compounds which are found to be orthorhombic with the parent $LiNiPO_4$. Morphology and grain sizes of the materials were investigated through FESEM. The FTIR technique was used to characterize the stretching and bending vibrational modes of different functional groups existing in the materials. The cathode properties were analysed through impedance spectroscopy and indicated on improved electrical properties of the doped samples as compared to the pure $LiNiPO_4$. The conductivity and modulus analyses of the samples were carried out at different temperatures and frequencies using the complex impedance spectroscopy technique.

Keywords: *lithium nickel phosphate, cathode materials, XRD, FTIR, modulus analysis*

I. Introduction

In recent years, lithium-ion batteries are the most promising power systems due to their high energy densities, long life cycle, environmental friendliness and safety. The olivine structured $LiMPO_4$ (M = Fe, Co, Mn and Ni) materials are examined as an attractive cathode materials due to their higher theoretical capacity and/or energy density than that of other commercial cathodes [1–7]. Among the four types $LiMPO_4$, $LiNiPO_4$ is expected to have the highest operating voltage (5.1 V), high energy density as well as the smallest volume change. However, the major drawback of the slow kinetics of the electronic and lithium ion transport for $LiNiPO_4$ cathodes restricts the development of $LiNiPO_4$. The performance of $LiNiPO_4$ can be improved by different synthesis methods, such as metal doping on the lattice and carbon coating on the particle surface [8,9]. However, the main approach is doping of metal ions on either Li^+ or Ni^{2+} lattice site which have been remarkably used by several researchers to improve the electronic conductivity of olivine type materials [10–14]. The electronic conductivity of $LiNiPO_4$ is found to increase with substitution of nickel ions with 10 at.% of Cu^{2+} and Mg^{2+}. So, it is of interest to study the effect of Mg^{2+} and Cu^{3+} doping on the electrical properties of $LiNiPO_4$. Hence, this paper aims to investigate the effect of Mg^{2+} and Cu^{3+} ion contents on the electrical properties of $LiNiPO_4$ and to study the different parameters at different temperatures by impedance spectroscopy.

II. Preparation and experimental techniques

The cathode compositions were synthesized by a solid-state reaction method from stoichiometric amounts of Li_2CO_3 (Merck 99.9%), NiO (Merck 99.9%), MgO (Merck 99.9%), CuO (Merck 99.9%) and $(NH_4)_3PO_4$ (Merck 99.9%). The solid state reaction synthesis involved three steps. In the first, the precursors, as raw materials, were well mixed and thoroughly

* Corresponding author: tel: + 91 98485 66927,
e-mail: *vijayababu.k@gmail.com*

Table 1. Lattice parameters, space group and cell volume for different compounds

Compound	*a* [Å]	*b* [Å]	*c* [Å]	Space group	Cell volume [Å^3]
$LiNi_{0.75}Mg_{0.25}PO_4$	10.0341	5.8762	4.6669	*Pnma*	275.1785
$LiNi_{0.75}Mg_{0.20}Cu_{0.05}PO_4$	10.0131	5.8794	4.6667	*Pnma*	274.7377
$LiNi_{0.75}Mg_{0.15}Cu_{0.10}PO_4$	9.9688	5.8745	4.6613	*Pnma*	272.98

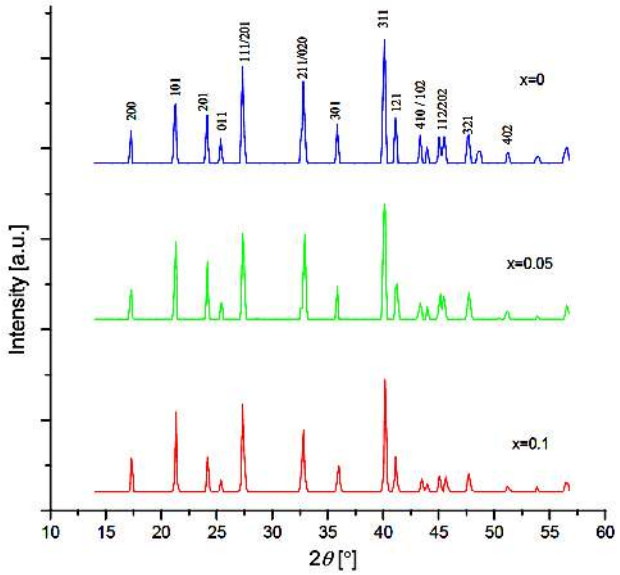

Figure 1. XRD patterns for $LiNi_{0.75}Mg_{0.25-x}Cu_xPO_4$ (x = 0, 0.05 and 0.1)

ground by using agate mortar and pestle, then subjected to heat treatment at a temperature of 120 °C for 12 hours and 500 °C for 4 hours to dry the samples and make them free from gases. The powder samples, with small amount of polyvinyl alcohol (PVA) as a binder, were ground and then pressed at 3 MPa pressure into a circular disk shaped pellet. The pellets were then sintered at 850 °C for 20 h in air at heating and cooling rates of 5 °C/min.

The powder X-ray diffraction (XRD) data of the prepared samples were collected on a Rigaku Cu-Kα diffractometer with diffraction angles of 20° and 80° in increments of 0.02°. The unit cell lattice parameters were obtained by the unitcell software from the 2θ and *hkl* values. Furthermore, the crystal size of the samples was determined from XRD pattern by applying the Scherrer's equation. The particle morphology of the powders were observed using a field effect scanning electron microscopy images taken from Carl Zeiss, EVOMA 15, Oxford Instruments, Inca Penta FETx3.JPG. Fourier transform infrared (FTIR) spectra were obtained on a Shimadzu FTIR-8900 spectrometer using KBr pellet technique in the wave number range between 400 and 1300 cm^{-1}. The impedance study was performed on the previously prepared sintered samples by a Hioki 3532-50 LCR Hitester in the frequency range 50 Hz to 5 MHz at temperature range from room temperature to 150 °C. The surface layers of the sintered pellet were carefully polished and washed in acetone and then the pellet was coated with silver paste on the opposite faces which acted as electrodes.

III. Results and discussion

X-ray diffraction

X-ray diffraction patterns of the prepared $LiNi_{0.75}Mg_{0.25-x}Cu_xPO_4$ (x = 0, 0.05 and 0.1) powders are shown in Fig. 1. The crystal phase of all the compounds are identified to be $LiNiPO_4$ phase with ordered olivine structure indexed by orthorhombic symmetry with *Pnma* space group. It can be seen from the patterns that all diffraction peaks are very sharp, which indicated that the samples have good crystal structure. There is no other phase except the orthorhombic $LiNiPO_4$, which means that entire copper ions entered the lattice of orthorhombic $LiNi_{0.75}Mg_{0.25}PO_4$. The main peaks for these prepared samples were labelled with *hkl* indexes (Fig. 1) [15–18]. It has been observed that the obtained 2θ values are in good agreement with JCPDS file number 88-1297.

The average crystallite size was calculated by the Debye-Scherrer method and found to be 67, 71 and 60 nm for $LiNi_{0.75}Mg_{0.25-x}Cu_xPO_4$ having x = 0, 0.05 and 0.1, respectively. The lattice parameters of all these samples have been calculated and summarized in Ta-

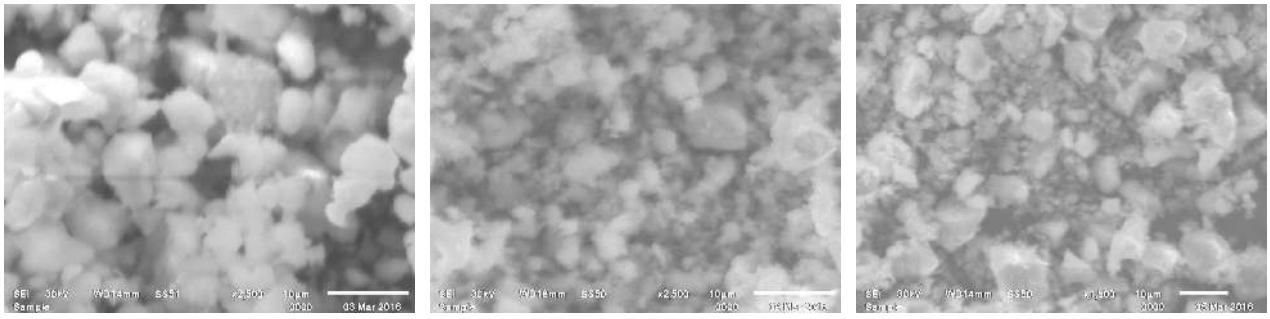

$LiNi_{0.75}Mg_{0.25}PO_4$ $LiNi_{0.75}Mg_{0.20}Cu_{0.05}PO_4$ $LiNi_{0.75}Mg_{0.15}Cu_{0.10}PO_4$

Figure 2. SEM images of prepared powders

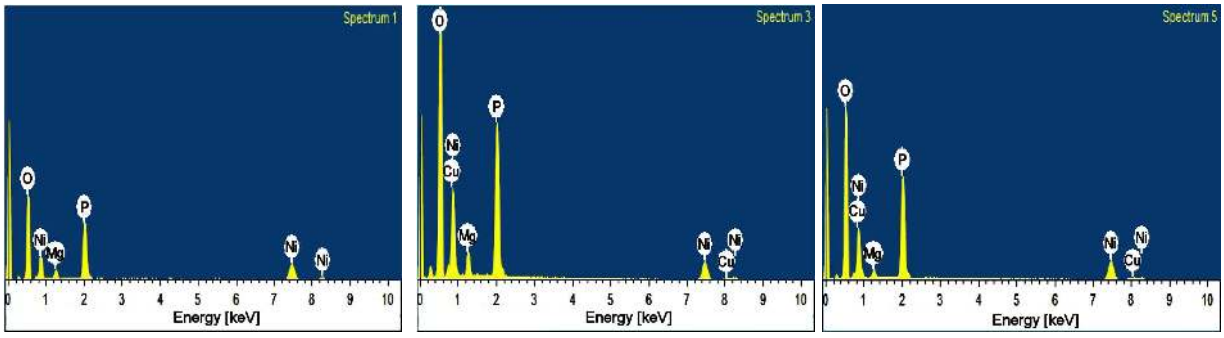

$LiNi_{0.75}Mg_{0.25}PO_4$ $LiNi_{0.75}Mg_{0.20}Cu_{0.05}PO_4$ $LiNi_{0.75}Mg_{0.15}Cu_{0.10}PO_4$

Figure 3. EDS spectra for different compounds

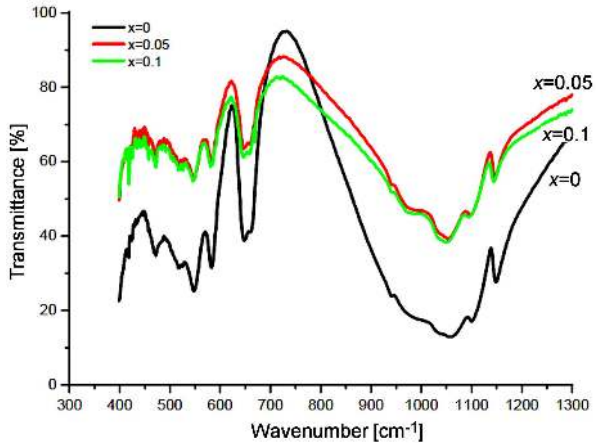

Figure 4. FTIR spectra for $LiNi_{0.75}Mg_{0.25-x}Cu_xPO_4$ (x = 0, 0.05 and 0.1)

ble 1. Increase or decrease of lattice parameters are depends on type and amount of doping ion. It has been seen that the lattice parameter along *b*-axis increases in $LiNiPO_4$ as the position of Ni^{2+} in the lattice is partially replaced by Mg^{2+}/Cu^{2+}, which is favourable to the transmission of lithium-ions for the lithium-ion transmitting along *b*-axis. The reason is that the ionic radius of Ni^{2+} (0.83 Å) is smaller than that of Cu^{2+} (0.87 Å) and it caused the increase of length of *b*-axis. The volume of the unit cell for Cu doped $LiNi_{0.75}Mg_{0.25}PO_4$ is larger than that of $LiNiPO_4$ which may be useful for lithium to insert and de-insert process [19–21].

FESEM with EDS

The microstructure of $LiNi_{0.75}Mg_{0.25-x}Cu_xPO_4$ (x = 0, 0.05 and 0.1) powders calcined at 800 °C is shown in Figure 2. The image clearly shows agglomeration of submicron size particles. The samples with Cu^{2+} and Mg^{2+} show different surface morphologies; $LiNi_{0.75}Mg_{0.25-x}Cu_xPO_4$ (x = 0, 0.05 and 0.1) consists of less agglomerated elongated particles. However, $LiNi_{0.75}Mg_{0.25}PO_4$ particles are hardly agglomerated and are not in regular shape [22–24].

EDS is used for the quantitative chemical analysis of the material, but it is unable to detect the elements with atomic number less than four. EDS spectra of $LiNi_{0.75}Mg_{0.25-x}Cu_xPO_4$ (x = 0, 0.05 and 0.1), presented in Fig. 3, show peaks corresponding to Ni, Mg, Cu, P and O elements present in the material and no other impurity is observed. It was not possible to detect Li due to the obvious reason that the X-ray fluorescence yield is extremely low for the elements H, He, Li and Be.

FTIR

The orthophosphates show main bands at 1060–1000 cm^{-1} and 580–520 cm^{-1}. Structure of phospho-olivine consists of LiO_6 and MO_6 octahedra linked to PO_4^{3-} polyanions. In $LiNiPO_4$ compounds, oxygen is bonded to three octahedral cations i.e., two M^{2+} and one Li^+ ion. Splitting of ν_3 components of PO_4^{3-} group, observed in phospho-olivine is due to type of bonding between oxygen and M octahedral cation. Although, the spectra are dominated by vibrational features due to phosphate ions, transition-metal ions also register their presence in the middle region around 400–700 cm^{-1}. The bands in the region of 700–850 cm^{-1} are due to phosphate groups such as $P_2O_7^{4-}$ or extended pyrophosphate structures [25,26]. The bands near 750 cm^{-1} indicate the presence of bridging P–O–P groups due to the impurity phase of pyrophosphates as shown in Fig. 4. The vibrational spectra data and band assignments of all the compounds are listed in Table 2.

Impedance spectroscopy

Impedance measurements are frequently used to characterize the electrical properties of materials and it

Table 2. Vibrational spectra data and band assignments

S.No	Infrared wavenumber [cm^{-1}]			Assignment
	x = 0	x = 0.05	x = 0.1	
1	457	448	449	ν (Li–O)
2	525	528	529	ν (Ni–O)
3	548	547	546	ν_2 (PO_4^{3-})
4	569	578	579	ν_2 (PO_4^{3-})
5	649	648	647	ν_4 (PO_4^{3-})
6	937	949	949	ν_1 (PO_4^{3-})
7	1060	1057	1054	ν_3 (PO_4^{3-})
8	1091	1094	1089	ν_3 (PO_4^{3-})
9	1139	1137	1139	ν_3 (PO_4^{3-})

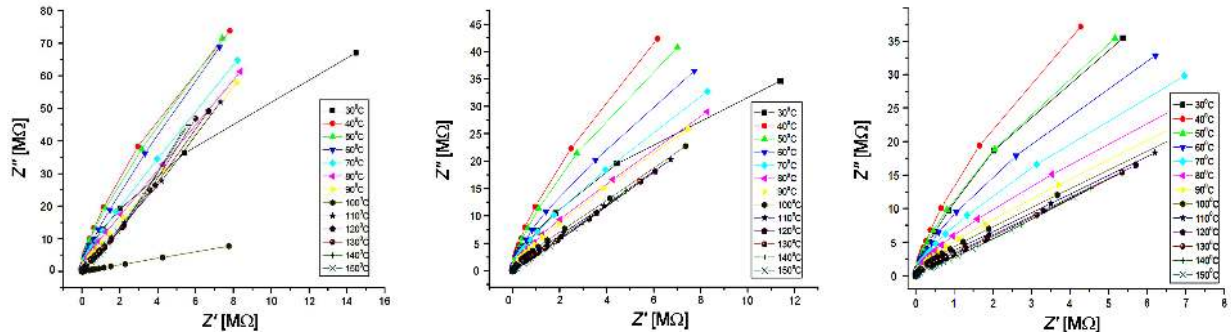

$LiNi_{0.75}Mg_{0.25}PO_4$ $LiNi_{0.75}Mg_{0.20}Cu_{0.05}PO_4$ $LiNi_{0.75}Mg_{0.15}Cu_{0.10}PO_4$

Figure 5. Nyquist plots at various temperatures for different compounds

has proven to be a powerful tool particularly for depicting the electrical conductivity of ionic, electronic and mixed ceramic materials. The frequency-dependent conductivity and dielectric permittivity studies provide important information on the ion transport and relaxation studies of fast ionic conductors. Thus, the complex impedance spectroscopic technique was used to analyse the electrical response of the polycrystalline samples in a wide range of frequencies. AC electrical data may be represented in any of the four basic formalisms which are interrelated to each other.

The measured impedance data can be represented in different forms, using the inter relations as follows:

$$Z^* = Z' - jZ'' \quad \text{complex impedance}$$
$$M^* = M' + jM'' = j\omega C_0 Z^* \quad \text{complex modulus}$$
$$\varepsilon^* = \varepsilon' - j\varepsilon'' \quad \text{complex permittivity}$$

where $j = \sqrt{-1}$, C_0 is the vacuum capacitance and $\omega = 2\pi f$ is the angular frequency. (Z', M', ε') and (Z'', M'', ε'') are the real and imaginary components of impedance, modulus and permittivity [27–29].

Figure 5 shows typical impedance diagrams of $LiNi_{0.75}Mg_{0.25-x}Cu_xPO_4$ (x = 0, 0.05 and 0.1) at different temperatures. The impedance spectrum comprises of an internal resistance of the material at high frequencies, a depressed semicircle at the middle frequencies, characteristic of a charge transfer process at interfaces or boundaries and a slope at low frequencies representing the diffusion process for the charge transport. The nature of the plots with the change in temperatures ensures a distinct effect on the characteristic impedance spectrum of the material by the appearance of single semicircular arc arising due to the bulk properties of the material. These semicircular arcs appear in distinct frequency ranges. This feature is almost similar at different temperatures, also with a difference in radii of curvature of the arcs, which reduces with rise in temperature. Nyquist plots show two semicircles indicating bulk and grain boundary contribution to the impedance behaviour for all temperatures. The semicircular pattern in the impedance spectrum is a representative of the electrical processes taking place in the material which can be expressed as an equivalent electrical circuit comprising of a parallel combination of resistive and capacitive elements. The presence of a semicircular arcs (i.e. the high frequency semicircle) arises due to the contribution of bulk properties of the material. The electrical processes taking place within the material has been modelled for a polycrystalline system. This provides convincing evidence that the electrical properties of $LiNi_{0.75}Mg_{0.25-x}Cu_xPO_4$ are dependent on microstructural as well as temperature [30–33].

The variations of real (Z') and imaginary (Z'') part of impedance with frequency at different temperatures of $LiNi_{0.75}Mg_{0.25-x}Cu_xPO_4$ (x = 0, 0.05 and 0.1) are shown in Figs. 6 and 7. The Z' and Z'' values decreased sharply with increase in frequency and display characteristic dispersion at lower temperatures. In addition, the Z' and Z'' values also decreased with the increase of

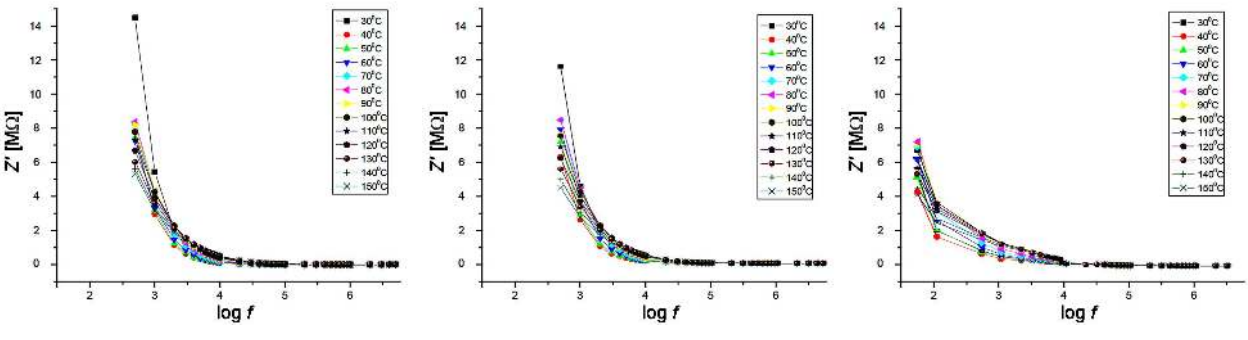

$LiNi_{0.75}Mg_{0.25}PO_4$ $LiNi_{0.75}Mg_{0.20}Cu_{0.05}PO_4$ $LiNi_{0.75}Mg_{0.15}Cu_{0.10}PO_4$

Figure 6. Variation of Z' with frequency for different compounds

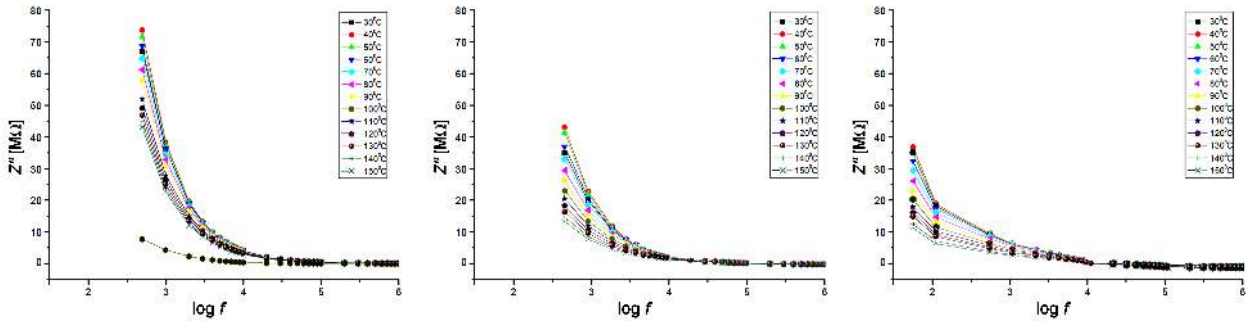

$LiNi_{0.75}Mg_{0.25}PO_4$ $LiNi_{0.75}Mg_{0.20}Cu_{0.05}PO_4$ $LiNi_{0.75}Mg_{0.15}Cu_{0.10}PO_4$

Figure 7. Variation of Z'' with frequency for different compounds

Cu^{2+} content. These observations indicate that there is a spread of relaxation time and the existence of a temperature dependent electrical relaxation phenomenon in the material [34,35].

AC Conductivity studies

The AC conductivity is calculated from dielectric data using the relation:

$$\sigma_{AC} = \omega \cdot \varepsilon_r \cdot \varepsilon_0 \cdot \tan\sigma$$

where $\omega = 2\pi f$. The variation of AC electrical conductivity of $LiNi_{0.75}Mg_{0.25-x}Cu_xPO_4$ (x = 0, 0.05 and 0.1) as a function of frequency at different temperatures is shown in Fig. 8. The conductivity spectrum displays characteristic conductivity dispersion throughout the frequency range below 150 °C, i.e. a low frequency independent plateau is observed, whereas in the higher frequency region dispersion of conductivity is still retained. The crossover from the frequency independent region to the frequency dependent regions shows the onset of the conductivity relaxation, indicating the transition from long range hopping to the short range ionic motion. The frequency of onset of conductivity relaxation shifts with temperature to higher frequency side. The highest conductivity was observed in the sample without copper ($LiNi_{0.75}Mg_{0.25}PO_4$), whereas in the copper substituted samples higher conductivity has the sample with x = 0.1 ($LiNi_{0.75}Mg_{0.15}Cu_{0.1}PO_4$). The decrease in conductivity is most probably due to the "anti-site" defect, where a small population of Li^+ and Ni^{2+} ions exchange their sites caused by the substitution of Ni^{2+} with a divalent ion [36,37]. The conductivity and activation energy values are listed in Table 3. It is shown that the conductivities of $LiNi_{0.75}Mg_{0.25}PO_4$, $LiNi_{0.75}Mg_{0.20}Cu_{0.05}PO_4$ and $LiNi_{0.75}Mg_{0.15}Cu_{0.1}PO_4$ at the room temperature are 2.95×10^{-9}, 2.83×10^{-9} and 2.86×10^{-9} S/cm, respectively, indicating that an increase of Cu doping concentration could definitely enhance the electronic conductivity and promote the Li storage performance.

Activation energy

The standard Arrhenius plots ($\log\sigma$ versus $1/T$) for all the prepared compounds are presented in Fig. 9 in accordance to the following equation:

$$\sigma = \sigma_0 \exp\left[-\frac{E_a}{k_B T}\right]$$

where E_a is the activation energy. These results show an increase of the conductivity with increasing temperature for all compounds indicating a characteristic activated behaviour over the complete temperature range studied. Furthermore, plots of $\log\sigma$ *vs.* $1/T$ are found to be linear in the range of temperatures above 350 K. The estimated values of E_a are 0.6522 eV, 0.7057 eV and 0.7645 eV for x = 0, 0.05 and 0.1 at 100 kHz, respectively. The type of temperature dependence of AC conductivity indicates that the electrical conduction in the material is a thermally activated process. It is well known that the motion of oxygen vacancies gives rise

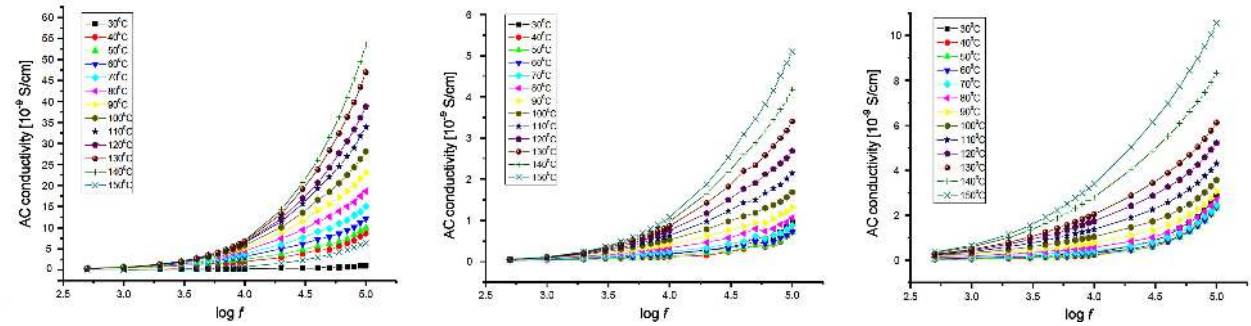

$LiNi_{0.75}Mg_{0.25}PO_4$ $LiNi_{0.75}Mg_{0.20}Cu_{0.05}PO_4$ $LiNi_{0.75}Mg_{0.15}Cu_{0.10}PO_4$

Figure 8. Variation of AC conductivity with frequency for different compounds

Table 3. Activation energies for different compounds at 100 kHz

Compound	AC conductivity at RT [S/cm]	Activation energy [eV]
$LiNi_{0.75}Mg_{0.25}PO_4$	2.95×10^{-9}	0.6522
$LiNi_{0.75}Mg_{0.20}Cu_{0.05}PO_4$	2.83×10^{-9}	0.7057
$LiNi_{0.75}Mg_{0.15}Cu_{0.10}PO_4$	2.86×10^{-9}	0.7645

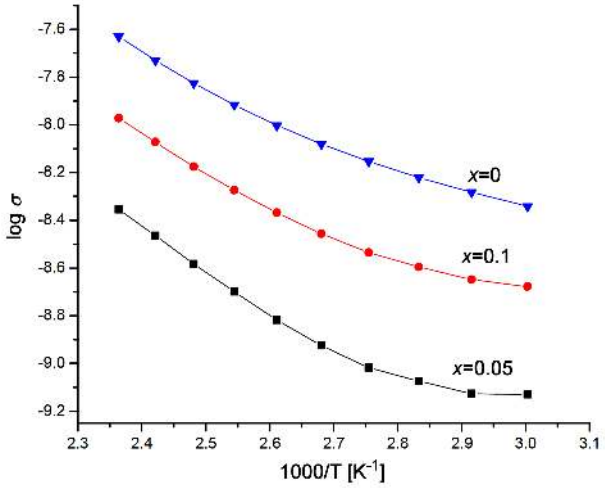

Figure 9. Arrhenius plots for different compounds

to activation energy of 1 eV. In cathode materials, usually oxygen vacancies are considered as one of the mobile charge carriers in olivine structure [38]. The ionization of oxygen vacancies creates conducting electrons, which are easily thermally activated. From the conduction results and the obtained activation energies it can be concluded that the conduction in the higher-temperature range is enhanced by the presence of oxygen vacancies.

Dielectric constant (ε')

Figure 10 shows the frequency dependence of dielectric constant (ε') at different temperature for the $LiNi_{0.75}Mg_{0.25-x}Cu_xPO_4$ (x = 0, 0.05 and 0.1) cathode materials. It is clear from this figure that ε' decreases with frequency and increases with temperature. The decrease of dielectric constant (ε') with frequency can be attributed to the fact that at low frequencies all four types of polarization, deformational (electronic and ionic) and relaxation (orientational and interfacial), are active and contribute to ε'. However, with the increase of frequencies the orientational polarization is less active in comparison to electronic and ionic polarization. This decreases the value of dielectric constant (ε') reaching a constant value at higher frequency [39,40].

The increase of dielectric constant (ε') with temperature can be attributed to the fact that the orientional polarization is related to the thermal motion of ions, so dipoles can be easily oriented at higher temperatures. Thus, when the temperature is increased the orientation of dipole is facilitated and this enables easier orientational polarization, which leads to increase of the dielectric constant (ε') with temperature. The degree of crystallinity also has influence on the dielectric constant.

Dielectric permittivity (ε'')

Figure 11 shows the variation of imaginary part of dielectric permittivity (ε'') with frequency for different compounds at different temperatures. Generally, for all samples ε'' decreases with frequency. The higher values of dielectric loss (ε'') at low frequency are due to the free charge motion within the materials. Dielectric loss increases in the lower frequency region in the samples with copper, reflecting the enhancement of mobility of charge carrier when Mg^{2+} is substitute with Cu^{2+}. Similar types of observations have been reported in literature [41].

Dielectric tangent loss ($\tan\delta$*)*

Figure 12 shows the variation of tangent loss with frequency of $LiNi_{0.75}Mg_{0.25-x}Cu_xPO_4$ (x = 0, 0.05 and 0.1) cathode materials at different temperatures. Dielectric tangent loss ($\tan\delta$) increases in the lower frequency region in the samples with copper, what is similar be-

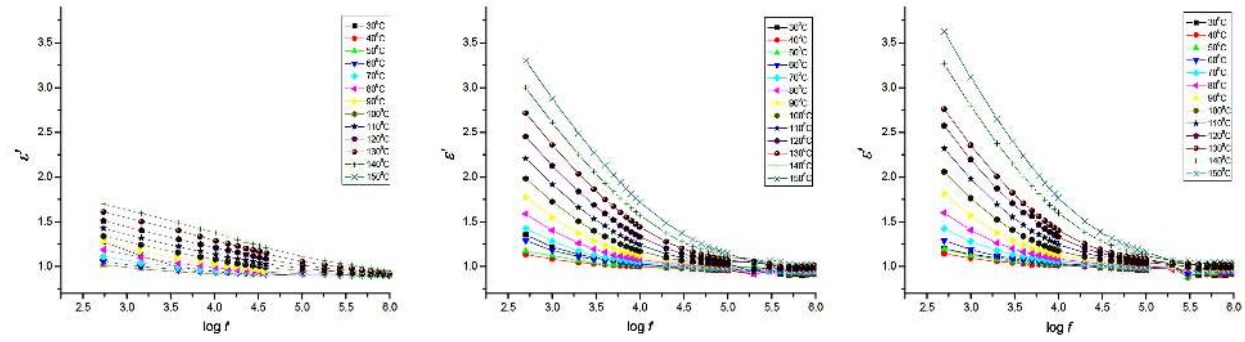

$LiNi_{0.75}Mg_{0.25}PO_4$ $LiNi_{0.75}Mg_{0.20}Cu_{0.05}PO_4$ $LiNi_{0.75}Mg_{0.15}Cu_{0.10}PO_4$

Figure 10. Variation of dielectric constant with temperature for different compounds

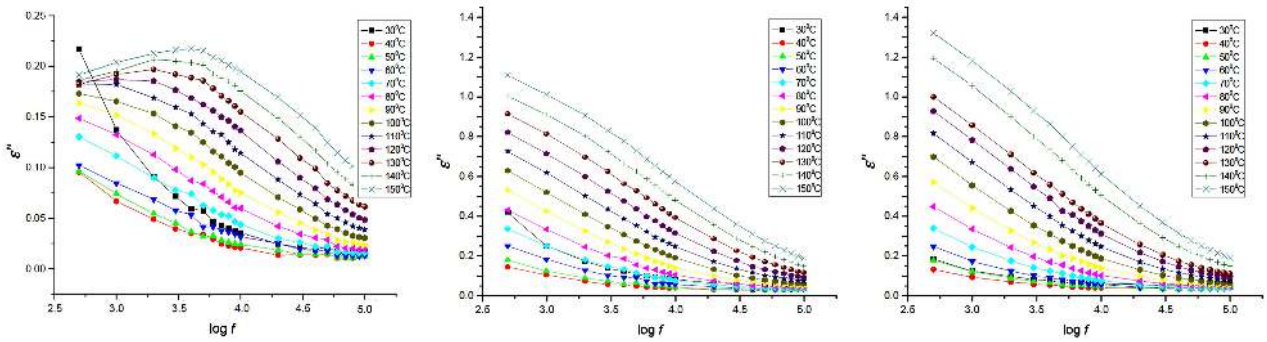

$LiNi_{0.75}Mg_{0.25}PO_4$ $LiNi_{0.75}Mg_{0.20}Cu_{0.05}PO_4$ $LiNi_{0.75}Mg_{0.15}Cu_{0.10}PO_4$

Figure 11. Variation of imaginary part of dielectric permittivity (ε'') *vs.* frequency for different compounds

haviour observed for dielectric loss (ε''). However, the tangent loss spectra are characterized with a peak appearing at the characteristic frequency for all samples, suggesting the presence of relaxing dipoles in the samples. The strength and frequency of relaxation depend on characteristic property of dipolar relaxation [42]. The tangent loss peaks shift towards higher temperatures for the defined sample composition. In addition, the tangent loss peaks shift towards the higher frequency with the increase in copper content (x value). It is believed that with addition of copper there is an increase in the amorphous content in the materials. The small and mobile diluents units speed up the segmental motion by increasing the available free volume, thereby reducing the relaxation time.

Electric modulus

The electrical response of the cathode materials can also be analysed using complex electric modulus. Complex impedance plots are more effective for the elements with the high resistance, but can also be useful for smallest capacitance elements. Using the complex electric modulus data the inhomogeneous nature of polycrystalline ceramics can be separated into bulk and grain boundary effects, which is sometime not clearly distinguished from complex impedance plots. One of the interesting advantages of the electric modulus formalism is that it suppresses the electrode effect. Figure 13 shows the real part of electric modulus M' *vs.* log f spectra obtained from 20 to 150 °C for the $LiNi_{0.75}Mg_{0.25-x}Cu_xPO_4$ samples.

From these plots, it is observed that the shape of each curve is non-Lorentzian type exhibiting a peak at the relaxation frequency with a long tail extending in the region of shorter relaxation time and a change in the value of peak height and the position of peak frequency were also observed for different doped materials [43].

IV. Conclusions

The paper investigates the structure and electrical properties of olivine structured $LiNi_{0.75}Mg_{0.25-x}Cu_xPO_4$ (x = 0, 0.05 and 0.1) cathode materials. The structural study was performed by X-ray powder diffraction and Fourier transforms infrared spectroscopy. The morphology of the surface and the grain sizes are analysed by scanning electron microscope. Impedance spectroscopy was used to establish microstructure-electrical properties relationship in the material. The crystal phase of all the compounds are identified to be $LiNiPO_4$ phase with ordered olivine structure indexed by orthorhombic symmetry with Pnma space group. The AC conductivity, dielectric constant and dielectric loss of the studied composition are investigated. Both the dielectric constant ε' and dielectric loss ε'' increase with temperature and decrease with frequency through the studied ranges. The dielectric constant may be attributed to orientation and space charge polarization respectively, whereas the tem-

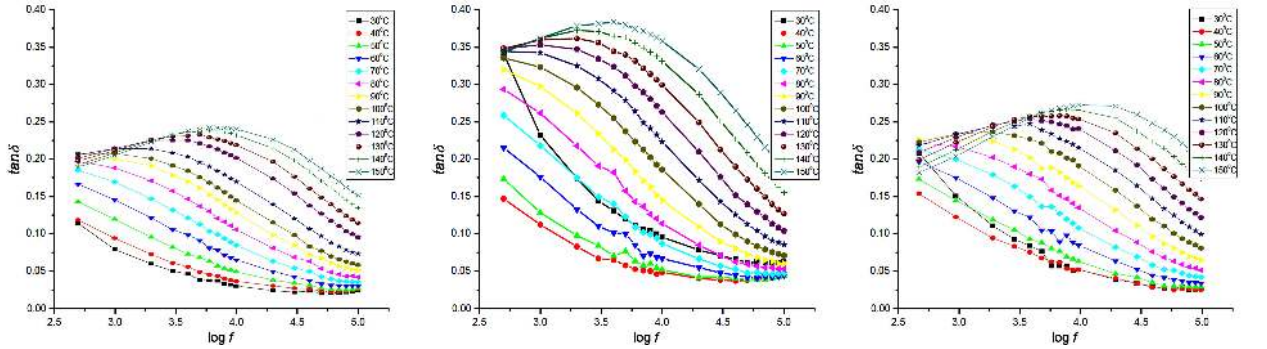

$LiNi_{0.75}Mg_{0.25}PO_4$ $LiNi_{0.75}Mg_{0.20}Cu_{0.05}PO_4$ $LiNi_{0.75}Mg_{0.15}Cu_{0.10}PO_4$

Figure 12. Variation of tan δ with temperature at different frequencies for different compounds

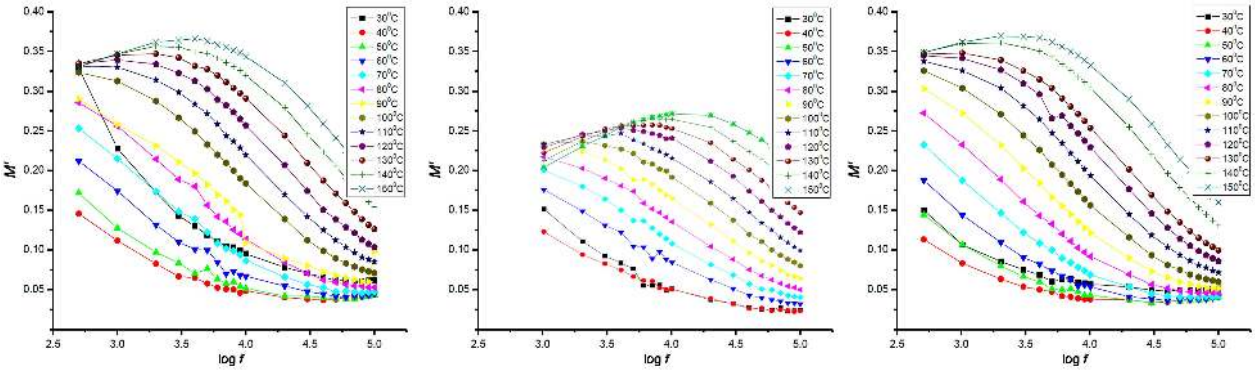

$LiNi_{0.75}Mg_{0.25}PO_4$ $LiNi_{0.75}Mg_{0.20}Cu_{0.05}PO_4$ $LiNi_{0.75}Mg_{0.15}Cu_{0.10}PO_4$

Figure 13. ***M′ vs.*** **frequency for different compounds**

perature dependence of the dielectric loss is associated with the conduction loss.

References

1. D. Bhuvaneswari, Gangulibabu, C.-H. Doh, N. Kalaiselvi, "Role of iron dopant and carbon additive in improving the ionic transport and electrochemical properties of $LiFe_xMn_{1-x}PO_4$ (x = 0.25 and 0.75) solid solutions", *Int. J. Electrochem. Sci.*, **6** (2011) 3714–3728.
2. J.M. Tarascon, M. Armand, "Issues and challenges facing rechargeable lithium batteries", *Nature*, **414** (2001) 359–367.
3. C.A.J. Fisher, V.M. Hart Prieto, M. Saiful Islam, "Lithium battery materials $LiMPO_4$ (M = Mn, Fe, Co, and Ni): Insights into defect association, transport mechanisms, and doping behavior", *Chem. Mater.*, **20** (2008) 5907–5915.
4. M. Minakshi, P. Singh, D. Appadoo, D.E. Martin, "Synthesis and characterization of olivine $LiNiPO_4$ for aqueous rechargeable battery", *Electrochim. Acta*, **56** (2011) 4356–4360.
5. G. Yang, H. Ni, H. Liu, P. Gao, H. Ji, S. Roy, J. Pinto, X. Jiang, "The doping effect on the crystal structure and electrochemical properties of $LiMn_xM_{1-x}PO_4$ (M = Mg, V, Fe, Co, Gd)", *J. Power Sources*, **196** (2011) 4747–4755.
6. S. Okada, S. Sawa, M. Egashira, J. Yamaki, M. Tabuchi, H. Kageyama, T. Konishi, A. Yoshino, "Cathode properties of phospho-olivine $LiMPO_4$ for lithium secondary batteries", *J. Power Sources*, **97-98** (2001) 430–432.
7. D. Morgan, A. Van der Ven, G. Ceder, "Li conductivity in Li_xMPO_4 (M = Mn, Fe, Co, Ni) olivine materials", *Electrochem. Solid-State Lett.*, **7** (2004) A30–A32.
8. D. Shanmukaraj, R. Murugan, "Synthesis and characterization of $LiNi_yCo_{1-y}PO_4$ (y = 0-1) cathode materials for lithium secondary batteries", *Ionics*, **10** (2004) 88–92.
9. A.K. Padhi, K.S. Nanjundaswamy, J.B. Goodenough, "Phospho-olivines as positive-electrode materials for rechargeable lithium batteries", *J. Electrochem. Soc.*, **144** (1997) 1188–1194.
10. J. Wolfenstine, J. Allen, "Ni^{3+}/Ni^{2+} redox potential in $LiNiPO_4$", *J. Power Sources*, **142** (2005) 389–390.
11. P. Muralidharan, M. Venkateswarlu, N. Satyanarayana, "Sol-gel synthesis, structural and ion transport studies of lithium borosilicate glasses", *Solid State Ionics*, **166** (2004) 27–38.
12. J. Su, B.Q. Wei, J.P. Rong, W.Y. Yin, Z.X. Ye, X.Q. Tian, L. Ren, M.H. Cao, C.W. Hu, "A general solution-chemistry route to the synthesis $LiMPO_4$ (M = Mn, Fe, and Co) nanocrystals with [010] orientation for lithium ion batteries", *J. Solid State Chem.*, **184** (2011) 2909–2919.
13. M. Broussely, P. Biensan, B. Simon, "Lithium insertion into host materials: the key to success for Li ion batteries", *Electrochim. Acta*, **45** (1999) 3–22.
14. J. Chen, M.J. Vacchio, S. Wang, N. Chernova, P.Y. Zavalij, M.S. Wittingham, "The hydrothermal synthesis and characterization of olivines and related compounds for electrochemical applications", *Solid State Ionics*, **178** (2008) 1676–1693.
15. A. Sanusi, S. Navaratnam, W.J. Basirun, "Synthesis of nanocrystalline olivine $LiNiPO_4$ powder prepared by sol-gel method: Thermal analysis and XRD studies", *Malaysian J. Anal. Sci.*, **18** (2014) 522–526.
16. Gangulibabu, D. Bhuvaneswari, N. Kalaiselvi, N. Jayaprakash, P. Periasamy, "CAM sol-gel synthesized $LiMPO_4$ (M = Co, Ni) cathodes for rechargeable lithium batteries", *J. Sol-Gel Sci. Technol.*, **49** (2009) 137–144.
17. R. Qinga, M.-C. Yang, Y.S. Meng, W. Sigmund, "Synthesis of $LiNi_xFe_{1-x}PO_4$ solid solution as cathode materials for lithium ion batteries", *Electrochim. Acta*, **108** (2013) 827–832.
18. M. Takahashi, S. Tobishima, K. Takei, Y. Sakurai, "Characterization of $LiFePO_4$ as the cathode material for rechargeable lithium batteries", *J. Power Sources*, **97-98** (2001) 508–511.
19. S.W. Kim, J. Kim, H. Gwon, K. Kang, "Phase stability study of $Li_{1-x}MnPO_4$ ($0 \leq x \leq 1$) cathode for Li-rechargeable battery", *J. Electrochem. Soc.*, **156** (2009) A635–A638.

20. Y. Iriyama, T. Kako, C. Yada, T. Abe, Z. Ogumi, "Charge transfer reaction at the lithium phosphorus oxynitride glass electrolyte/lithium cobalt oxide thin film interface", *Solid State Ionics*, **176** (2005) 2395–2398.
21. T. Muraliganth, A. Manthiram, "Understanding the shifts in the redox potentials of olivine $LiM_{1-y}M_yPO_4$ (M = Fe, Mn, Co and Mg) solid solutions cathodes", *J. Phys. Chem. C*, **114** (2010) 15530–15540.
22. K. Amine, H. Yasuda, M. Yamachi, "Olivine $LiCoPO_4$ as 4.8 V electrode materials for lithium batteries", *Solid State Lett.*, **3** (2000) 178–179.
23. V. Koleva, R. Stoyanova, E. Zhecheva, "Formation of metastable Na_2CrO_4-type $LiNiPO_4$ from a phosphate-formate precursor", *Eur. J. Inorg. Chem.*, **1** (2010) 127–131.
24. C. Julien, M.A. Camacho-Lopez, T. Mohan, S. Chitra, P. Kalyani, S. Gopukumar, "Combustion synthesis and characterization of substituted lithium cobalt oxides in lithium batteries", *Solid State Ionics*, **135** (2000) 241–248.
25. A. Ait Salah, P. Jozwiak, J. Garbarczyk, K. Benkhouja, K. Zaghib, F. Gendron, C.M. Julien, "Local structure and redox energies of lithium phosphates with olivine-and Nasicon-like structures", *J. Power Sources*, **140** (2005) 370–375.
26. A. Rouier, G.A. Nazri, C. Julian, "Vibrational spectroscopy and electrochemical properties of $LiNi_{0.7}Co_{0.3}O_2$ cathode material for rechargeable lithium batteries", *Ionics*, **3** (1997) 170–176.
27. J.R. Macdonald, *Impedance Spectroscopy*, Wiley, New York, 1987.
28. J.T.C. Irvine, D.C. Sinclair, A.R. West, "Electroceramics: characterization by impedance spectroscopy", *Adv. Mater.*, **2** (1990) 138–140.
29. B. Ellis, P.S. Herle, Y.H. Rho, L.F. Nazar, R. Dunlap, L.K. Perry, D.H. Ryan, "Nanostructured materials for lithium-ion batteries: Surface conductivity vs. bulk ion/electron transport", *Faraday Discuss.*, **134** (2007) 119–141.
30. P. Wilk, J. Marzec, J. Molenda, "Structural and electrical properties of $LiNi_{1-y}Co_yO_2$", *Solid State Ionics*, **157** (2003) 109–114.
31. O. Bohnke, J. Emery, J.L. Fourquet, "Anomalies in Li^+ ion dynamics observed by impedance spectroscopy and ^7Li NMR in the perovskite fast ion conductor $(Li_{3x}La_{2/3-x}\square_{1/3-2x})TiO_3$", *Solid State Ionics*, **158** (2003) 119–132.
32. K. Rissouli, K. Benkhouja, J.R. Ramos-Barrado, C. Julien, "Electrical conductivity in lithium orthophosphates", *Mater. Sci. Eng. B*, **98** (2003) 185–189.
33. M. Ben Bechir, A. Ben Rhaiem, K. Guidara, "AC conductivity and dielectric study of $LiNiPO_4$ synthesized by solid state method", *Bull. Mater. Sci.*, **37** (2014) 1–8.
34. C.M. Julien, A. Mauger, K. Zaghib, R. Veillette, H. Groult, "Structural and electronic properties of the $LiNiPO_4$ orthophosphate", *Ionics*, **18** (2012) 625–633.
35. M.A.G. Aranda, S. Bruque, J.R. Ramos-Barrado, J.P. Attfield, "Relation between structure and ionic conductivity in the lithium derivatives, $LiMnXO_4(OH)$ (X = P, As)", *Solid State Ionics*, **63-65** (1993) 407–410.
36. M. Prabhu, S. Selvasekarapandian, A.R. Kulkarni, S. Karthikeyan, C. Sanjeeviraja, "Influence of europium doping on conductivity of $LiNiPO_4$", *Trans. Nonferrous Met. Soc. China*, **22** (2012) 342–347.
37. A. Ben Rhaiem, F. Hlel, K. Guidara, M. Gargouri, "Electrical conductivity and dielectric analysis of $AgNaZnP_2O_7$ compound", *J. Alloys Compd.*, **485** (2009) 718–723.
38. B. Jin, H.-B. Gu, "Preparation and characterization of $LiFePO_4$ cathode materials by hydrothermal method", *Solid State Ionics*, **178** (2008) 1907–1914.
39. S.S.N. Bharadwaja, S.B. Krupanidhi, "Study of AC electrical properties in multigrain antiferroelectric lead zirconate thin films", *Thin Solid Films*, **391** (2001) 126–130.
40. A. Orliukas, A. Dindune, Z. Kanepe, "Synthesis, structure and peculiarities of ionic transport of $Li_{1.6}Mg_{0.3}Ti_{1.7}(PO_4)_3$ ceramics", *Solid State Ionics*, **157** (2003) 177–181.
41. M. Prabu, S. Selvasekarapandian, A.R. Kulkarni, S. Karthikeyan, G. Hirankumar, C. Sanjeeviraja, "Structural, dielectric, and conductivity studies of yttrium-doped $LiNiPO_4$ cathode materials", *Ionics*, **17** (2011) 201–207.
42. C.T. Moynihan, L.P. Bosech, N.L. Laberge, "Decay function for the electric field relaxation in vitreous ionic conductors", *Phys. Chem. Glass*, **14** (1973) 122–125.
43. R. Selwin Joseyphus, E. Viswanathan, C. Justin Dhanaraj, J. Joseph, "Dielectric properties and conductivity studies of some tetradentate cobalt(II), nickel(II), and copper(II) Schiff base complexes", *J. King Saud University Sci.*, **24** (2012) 233–236.